



Epimedium koreanum Nakai-Induced Liver Injury—A Mechanistic Study Using Untargeted Metabolomics

Pin Li, Lin Zhang*, Zhaojuan Guo, Qianjun Kang, Cong Chen, Xiaoyao Liu, Quantao Ma, Jingxuan Zhang, Yujie Hu and Ting Wang*

Beijing Institute of Traditional Chinese Medicine, Beijing University of Chinese Medicine, Beijing, China

OPEN ACCESS

Edited by:

Shuai Ji,
Xuzhou Medical University, China

Reviewed by:

Zhilei Wang,
Chengdu University of Traditional
Chinese Medicine, China
Li Chao,
Shandong First Medical University,
China

*Correspondence:

Lin Zhang
zlbucm@163.com
Ting Wang
wangting1973@sina.com

Specialty section:

This article was submitted to
Ethnopharmacology,
a section of the journal
Frontiers in Pharmacology

Received: 02 May 2022

Accepted: 30 May 2022

Published: 13 July 2022

Citation:

Li P, Zhang L, Guo Z, Kang Q, Chen C,
Liu X, Ma Q, Zhang J, Hu Y and Wang T
(2022) Epimedium koreanum
Nakai-Induced Liver Injury—A
Mechanistic Study Using
Untargeted Metabolomics.
Front. Pharmacol. 13:934057.
doi: 10.3389/fphar.2022.934057

Epimedium Folium is widely used worldwide as an herbal supplement, and the risk of its induced liver damage has emerged in recent years. Our preliminary study has found that, among several Epimedium Folium species specified in the Chinese Pharmacopoeia, *Epimedium koreanum* Nakai has a more severe propensity for hepatotoxicity. However, the mechanism of hepatotoxicity of *Epimedium koreanum* Nakai is still unclear. In this study, untargeted metabolomics was performed to analyze the serum and liver tissue to explore the mechanism of hepatotoxicity of *Epimedium koreanum* Nakai. The results of experiments *in vivo* showed that, after 28 days of exposure to *Epimedium koreanum* Nakai ethanol extract (EEE), the liver weight, levels of AST, ALP, TBIL, etc. in serum of rats in the EEE group were significantly increased, as well as severe cytoplasmic vacuolation appeared in the liver tissue, which suggested that EEE has significant hepatotoxicity. Subsequently, the results of metabolomics revealed significant changes in the metabolic profile in the liver and serum of rats after EEE exposure, in which metabolites in serum such as flavin mononucleotide, phenylacetylglycine, glutathione, L-tryptophan, and sphingomyelin were able to accurately identify liver injury caused by EEE and could be used as serum markers to reflect EEE-induced liver injury. The KEGG pathway enrichment analysis revealed that EEE caused extensive effects on rats' metabolic pathways. Some of the most affected pathways included glutathione metabolism, glutamate metabolism pathway, primary bile acid biosynthesis pathway, and sphingolipid metabolism pathway, which were all directed to the biological process of ferroptosis. Then, the main markers related to ferroptosis in the liver were examined, and the results demonstrated that the content of malondialdehyde was significantly increased, the activity of superoxide dismutase was significantly reduced, the ferroptosis inhibitory proteins GPX4 and System x_c^- were significantly downregulated, and the ferroptosis-promoting protein ACSL4 was significantly up-regulated. Judging from these results, we concluded that the mechanism of hepatotoxicity of *Epimedium koreanum* Nakai was probably related to the induction of ferroptosis in hepatocytes.

Keywords: herb-induced liver injury, Epimedium koreanum Nakai, metabolomics, glutathione, ferroptosis

INTRODUCTION

Epimedium Folium (Yinyanghuo in Chinese) is the dried leaf of *Epimedium brevicornu* Maxim., *Epimedium sagittatum* (Siebold&Zucc.) Maxim., or *Epimedium pubescens* Maxim. or *Epimedium koreanum* Nakai, in the family berberidaceae (Chinese Pharmacopoeia Commission, 2020). In the theory of Traditional Chinese Medicine, Epimedium Folium has the ability to dispel wind and cold, tonify the kidneys, and strengthen the tendons (Ma et al., 2011). It is widely used to treat various diseases, such as osteoporosis, impotence, infertility, cardiovascular disease, and amnesia (Ma et al., 2011). However, in recent years, two registered drugs with Epimedium Folium as the main ingredient, Zhuangguguanjie Pill and Xianlinggubao Capsules, were reported to be associated with liver injury in humans in clinical applications (Cheng et al., 2013; Tang et al., 2017; Tang et al., 2018; Wu et al., 2019), which has attracted widespread attention. Drug-induced liver injury is one of the most serious and common adverse drug reactions in clinical practice (Navarro et al., 2017), and severe liver injury may induce acute liver failure in patients and even lead to the death of patients (Tujios and Fontana, 2011; Iorga et al., 2017). Therefore, it is important to investigate the potential risk of liver injury of Epimedium Folium. At present, the research on the hepatotoxicity of Epimedium Folium has been gradually carried out. Some researchers have found that Icariside I and Icariside II (the main components of Epimedium Folium) could induce specific hepatotoxicity by enhancing the activation of nlrp3 inflammasome (Wang Z et al., 2020; Gao et al., 2021). Other researchers also have found that both 2''-O-rhamnosylcariside II and Sagittatoside B caused severe hepatocyte vacuolation and hepatocyte degeneration in adult zebrafish after 15 consecutive days of treatment (Zhong et al., 2019). However, there are few studies on the mechanism of Epimedium Folium inducing hepatotoxicity *in vivo*.

Most of the liver injury caused by Chinese herbal medicine *in vivo* is extremely complex and shows significant individual differences (García-Cortés et al., 2016; Brown, 2017). Metabolomics reveals the intrinsic mechanisms of growth and development, disease, and environmental influences on the body through a comprehensive and systematic analysis of metabolites in body fluids, tissues, or cells (Gong et al., 2017; Gika et al., 2019), which has been increasingly applied in exploring the mechanism of hepatotoxicity of herbal medicines (Duan et al., 2018). Zhaoyan Zhang et al. found that Polygoni Multiflori Radix extracts could cause liver damage by interfering with α -linolenic acid metabolism, taurine and taurine metabolism, glycerophospholipid metabolism, and primary bile acid biosynthetic pathways based on a metabolomic approach (Zhang et al., 2019). Yusha Luo et al. found that gardenia might cause liver injury by disrupting pyrimidine, purine, and amino acid metabolism and pantothenic acid and Coenzyme A biosynthesis through metabolomic methods (Luo et al., 2021). Applying metabolomics to study the hepatotoxicity of Epimedium Folium can help not only to clarify the toxicological characteristics of Epimedium Folium but also to reveal its potential mechanism.

In a previous study, we have found that *Epimedium koreanum* Nakai had more severe hepatotoxicity among several Epimedium Folium prescribed in the Chinese Pharmacopoeia, and its mechanism of hepatotoxicity was considered to be related to oxidative stress by experiments *in vitro* (Zhang L et al., 2020). However, the detailed mechanism of liver injury caused by *Epimedium koreanum* Nakai *in vivo* has not been elucidated. Based on the status of the prophase management research, we planned to study the mechanism of hepatotoxicity of *Epimedium koreanum* Nakai in this study by hepatotoxicity evaluation *in vivo* and non-targeted metabolomics method. The hepatotoxicity of *Epimedium koreanum* Nakai ethanol extract (EEE) was first investigated and validated by histopathological and biochemical methods, and the serum and liver samples were analyzed by untargeted metabolomics. Then, the differential metabolites of these samples were identified and screened using the UPLC-Q-TOF/MS technology platform and were analyzed to predict the pathways of EEE-induced liver injury *in vivo*. Subsequently, the mechanisms were investigated and analyzed by detecting key indicators in the pathway. This study could provide a reference for the safe utilization of Epimedium Folium in clinical practice.

MATERIALS AND METHODS

Chemicals and Reagents

Methanol and acetonitrile (UHPLC grade) were purchased from Fisher Chemical (Darmstadt, Germany). Ammonium acetate (70221) and sodium pentobarbital (P3761) were purchased from Sigma-Aldrich (St. Louis, Missouri, United States). Icaritin (110737-201516, purity >98%) and epimedin C (111780-201503, purity >98%) were purchased from the National Medical Products Administration (Beijing, China). Epimedin A (C15J3G1, purity >98%), epimedin B (C28S3G1, purity >98%), epimedin C (H16D5X1, purity >98%), and baohuoside I (H16D5X1, purity >98%) were purchased from Shanghai yuanye Bio-Technology Co., Ltd. (Shanghai, China). Alkaline phosphatase (ALP, AUZ8511), alanine transaminase (ALT, AUZ9151), aspartate aminotransferase (AST, AUZ9022), direct bilirubin (DBIL, AUZ9056), and total bilirubin (TBIL, AUZ8613) assay kits were purchased from Beckman Coulter (Suzhou, China). The malondialdehyde (MDA, M496) assay kit was purchased from Dongren Chemical Technology Co., Ltd. (Shanghai, China). The superoxide dismutase (SOD, S0101S) activity assay kit was purchased from Beyotime Biotechnology (Shanghai, China). *Epimedium koreanum* Nakai was obtained from the backup samples of previous experiments in our laboratory's herbal sample collection room (Zhang L et al., 2020).

EEE was produced by extracting dried *Epimedium koreanum* Nakai twice with 10 volumes of 70% ethanol-water (V/V), and the extract solution from both times was filtered and concentrated at 50 °C under negative pressure. The concentrates were freeze-dried to obtain a brown extract, and the ratio of the obtained extract from the original herb was 35.2%.

Quality Assessment of *Epimedium koreanum* Nakai Ethanol Extract

To evaluate the quality of EEE, we determined the concentrations of the five main components in EEE using high-performance liquid chromatography (HPLC). Standard solutions preparation: a mixed standard solution of icaritin, epimedin C, epimedin A, epimedin B, epimedin C, and baohuoside I was prepared using 50% DMSO: H₂O solution with the concentrations of 11.1 µg/ml, 12.5 µg/ml, 22.9 µg/ml, 12.1 µg/ml, and 9.4 µg/ml for each compound.

Sample solution preparation: 0.5 g EEE was added into 100 ml 50% DMSO: H₂O solution (V/V) and sonicated for 30 min to dissolve fully. After cooling to room temperature, the solution was filtered using a 0.45 µm membrane to obtain the sample solution.

The HPLC method used for the detection was described in the following way: C₁₈ column (Platisil, 4.6 mm × 250 mm, 5 µm, Decima Technology Co., Ltd., Beijing, China). The mobile phase was acetonitrile (A): water (B), and the procedure of gradient elution was (time/A%): 0–25 min, 25%–27%; 25–45 min, 27%–49%; 45–65 min, 49%–81%. The chromatographic analysis was performed with the column temperature maintained at 25°C, mobile phase flow rate at 1 ml/min, detection wavelength at 277 nm, and sample injection volume of 10 µl.

Animals Handling and Experimental Design

Male Sprague Dawley rats (180–200 g) were purchased from Beijing Vital River Laboratory Animal Technology Co., Ltd (license number SCXK-[jing] 2016-0011). The rats used for the experiments were housed at the Animal Experiment Center of Beijing University of Chinese Medicine, where room temperature was maintained at 20 ± 2°C and humidity at 60–70%, and a 12-h light/dark cycle was maintained. Rats had free access to a standard diet and water throughout the experimental period. All rats were acclimatized to this environment for 4 days before the experiment.

After acclimatization, the experimental rats were randomly divided into control and EEE groups ($n = 6$, each group). EEE was processed as solutions with deionized water before being used. The EEE group was administered EEE solution at 2 g original herb/kg (0.704 g EEE/kg) for 28 days, in a volume of 1 ml/100 g, once a day. The dosage of EEE was based on our previous studies (Zhang et al., 2018). The control group was also given an equal amount of purified water. Throughout the experiment, all rats were unfettered access to water and food and were weighed every 7 days. On the 28th day, 2 h after the administration, the rats were anesthetized intraperitoneally with sodium pentobarbital, blood were collected from the abdominal aorta to prepare serum samples, and liver tissues were dissected and collected. The study protocol was carried out under the approval and supervision of the Center for Experimental Animal Welfare and Ethics of Beijing University of Traditional Chinese Medicine.

Serum Biochemical Analysis

Blood from rats was collected in 5 ml Vacutainer tubes and then centrifuged for 15 min (1,500 g, 4°C) to collect the upper serum layer as serum samples. Liver injury was assessed by measuring

AST, ALT, ALP, DBIL, and TBIL in each rat serum sample using CX4 Pro automated biochemical analyzer (Beckman, Brea, CA, United States) according to the manufacturer's instructions.

Organ Weight and Histopathological Assessment

After dissection, the livers and brains of the rats were immediately harvested and weighed after washing with normal saline and wiping dry. Part of rat liver tissue was fixed with 10% neutral formalin for 48–72 h, dehydrated, embedded in paraffin, sectioned, stained with hematoxylin and eosin (H&E), and the pathological changes of liver tissues were observed under the microscope. The remaining livers were kept at –80°C for metabolomics, western blot, MDA, and SOD analysis.

Preparation of Liver and Serum Metabolisms Samples

In addition to using for histopathological assessment, the rest of the liver tissues were immediately frozen in liquid nitrogen and stored at –80 °C. For UPLC-Q-TOF/MS analysis, liver tissues were cut on dry ice, and 100 mg were weighed precisely into Eppendorf tubes (2 ml) with 1 ml of pre-chilled methanol: acetonitrile: water (2:2:1, v/v), which were homogenized and broken by a homogenizer. The homogenate was centrifuged for 15 min (14,000 g, 4°C), and 900 µl of supernatant from each tube was placed in a new Eppendorf tube and dried in a vacuum centrifuge as the test sample. The samples were redissolved in 100 µl of acetonitrile/water (1:1, v/v) solvent for UPLC-Q-TOF/MS analysis.

The rest of the serum samples were aspirated and placed in Eppendorf tubes (2 ml) frozen in liquid nitrogen and stored at –80°C. For UPLC-Q-TOF/MS analysis, serum samples were slowly thawed at 4°C, and 100 µl aliquots were vortexed with 400 µl cold methanol/acetonitrile (1:1, v/v) incubating at –20°C for 30 min to remove proteins. The mixture was centrifuged for 15 min (14,000 g, 4°C), and 400 µl of supernatant from each tube was placed in a new tube and dried under a vacuum. The samples were redissolved in 100 µl of acetonitrile/water (1:1, v/v) solvent for UPLC-Q-TOF/MS analysis.

UPLC-Q-TOF/MS Analysis

Samples were analyzed using UPLC (1,290 Infinity LC, Agilent Technologies) coupled with quadrupole time-of-flight (AB Sciex Triple TOF 6600). For HILIC separation, a 2.1 mm × 100 mm ACQUIY UPLC BEH 1.7 µm column (Waters, Ireland) was used. In the positive and negative ESI modes, the mobile phases contained 25 mM ammonium acetate and 25 mM ammonium hydroxide aqueous solution (A) and acetonitrile (B). The gradient elution procedure was as follows (time/B): 0–0.5 min, 95%; 0.5–7 min, 95%–65%; 7–8 min, 65%–40%; 8–9 min, 40%; 9–9.1 min, 40%–95%; 9.1–12 min, 95%. The samples were placed in a 4°C autosampler throughout the analysis. To avoid the effects of fluctuations in the instrument detection signal, samples were analyzed continuously in random order. QC samples were inserted in the sample queue to monitor and

evaluate the stability of the system and the reliability of the experimental data. The gradient flow rate was 0.3 ml/min, and the column temperature was kept constant at 25°C. A 2 µl aliquot of each sample was injected.

For mass spectrum (MS) analysis, the AB Triple TOF 6600 mass spectrometer was used for the acquisition of primary and secondary spectra of the samples. The ESI source conditions after BEH Amide chromatographic separation were as follows: Ion Source Gas1 (Gas1): 60, Ion Source Gas2 (Gas2): 60, Curtain gas (CUR): 30, source temperature: 600°C, IonSapary Voltage Floating (ISVF) ± 5500 V (positive and negative modes); TOF MS scan m/z range: 60–1,000 Da, product ion scan m/z range: 60–1,000 Da, product ion scan m/z range: 25–1,000 Da, TOF MS scan accumulation time 0.20 s/spectra, product ion scan accumulation time 0.05 s/spectra; secondary mass spectra were obtained using information. The secondary mass spectra were acquired using information-dependent acquisition (IDA) and high sensitivity mode, Declustering potential (DP): ±60 V (positive and negative modes), Collision Energy: 35 ± 15 eV, IDA settings as follows Exclude isotopes within 4 Da, Candidate ions to monitor per cycle: 10.

Data Extraction and Multivariate Analysis

Raw data of UPLC-Q-TOF/MS in Wiff format were converted to mzXML format using ProteoWizard, and then XCMS software was used for peak alignment, retention time correction, and extraction of peak areas. In the extracted ion features, only those with more than 50% of non-zero measurements were retained. Compound identification of metabolites was performed by comparing accurate m/z values (<10 ppm) and MS/MS spectra with an in-house database built from available authentic standards.

After normalizing the processed data to the total peak intensity, pre-to-scale principal component analysis (PCA) and orthogonal partial least squares discriminant analysis (OPLS-DA) multivariate data analysis were performed using the R package (ropls) (Thévenot et al., 2015).

Metabolic Pathways Analysis and Metabolic Fingerprints Identification

Metabolites obtained from metabolome analysis, with VIP >1 in the OPLS-DA analysis, were further applied to Student's t-test. Metabolites, that *p*-value < 0.05 and VIP >1, were selected as candidate biomarkers. Pathway analysis of candidate biomarkers was performed using MetaboAnalyst 5.0. The predictive performance of potential biomarkers for liver toxicity was analyzed using receiver operating characteristic curves (ROC) to establish metabolic fingerprints.

Western Blotting, MDA, and SOD Analysis

Liver tissue, which was kept at –80°C for western blotting, was cut on dry ice, an appropriate amount of liver tissue was weighed, RIPA protein extract was added, and then fully disrupted with a tissue homogenizer, and then placed on ice for 10 min. Then the supernatant was collected by centrifugation (14,000 g, 4°C) for 30 min. The protein concentration was assessed by using the BCA protein assay kit. Electrophoresis was performed by using

10% sodium dodecyl sulphate polyacrylamide gel electrophoresis (SDS-PAGE) to separate the proteins. After electrophoresis, proteins were transferred onto polyvinylidene fluoride (PVDF) membranes using a semi-dry method. The PVDF membranes were immersed in 5% TBST skim milk powder solution for 60 min at room temperature for non-specific closure. Then the PVDF membranes were then incubated for 12 h at 4 °C with the following primary antibodies: anti-GPX4 antibody (ab125066, Abcam, Cambridge, UK; 1:20,000), anti-ACSL4 antibody (ab155282, Abcam; 1:10,000), anti-System x_c⁻ antibody (ab175186, Abcam; 1:20,000), anti GAPDH antibody (ab9485, Abcam; 1:5,000). After the primary antibody incubation was completed, the PVDF membrane was washed 3 times with TBST, then incubated with hrp-labeled secondary antibody for 1 h at room temperature, and then the PVDF membrane was washed three times with TBST, 5 min each time. Add ECL-plus chemistry and incubate. The film was exposed using an Amersham Imager 680 blot and gel imager, and the grayscale values of the protein bands were analyzed. MDA content in rat liver tissue was assayed according to the manufacturer's instructions, as well as SOD activity.

Statistical Analysis

Experimental data were expressed as mean ± standard deviation (SD), and statistical analysis of data was performed using GraphPad Prism software (version 8.0). *p*-values of <0.05 (*), ≤0.01 (**) were adopted for statistical significance. Bodyweight, liver weight, liver/brain weight ratio, liver/body weight ratio, AST, ALP, TBIL, SOD, MDA, and Western blot data were analyzed using Student's t-test. All mass spectrometry data were processed by XCMS for peak alignment, retention time correction, and extraction of peak areas. The intensity of each ion was normalized according to the total ion count. PCA and OPLS-DA were performed using the R package (ropls). Pathway analysis was performed based on MetaboAnalyst 5.0.

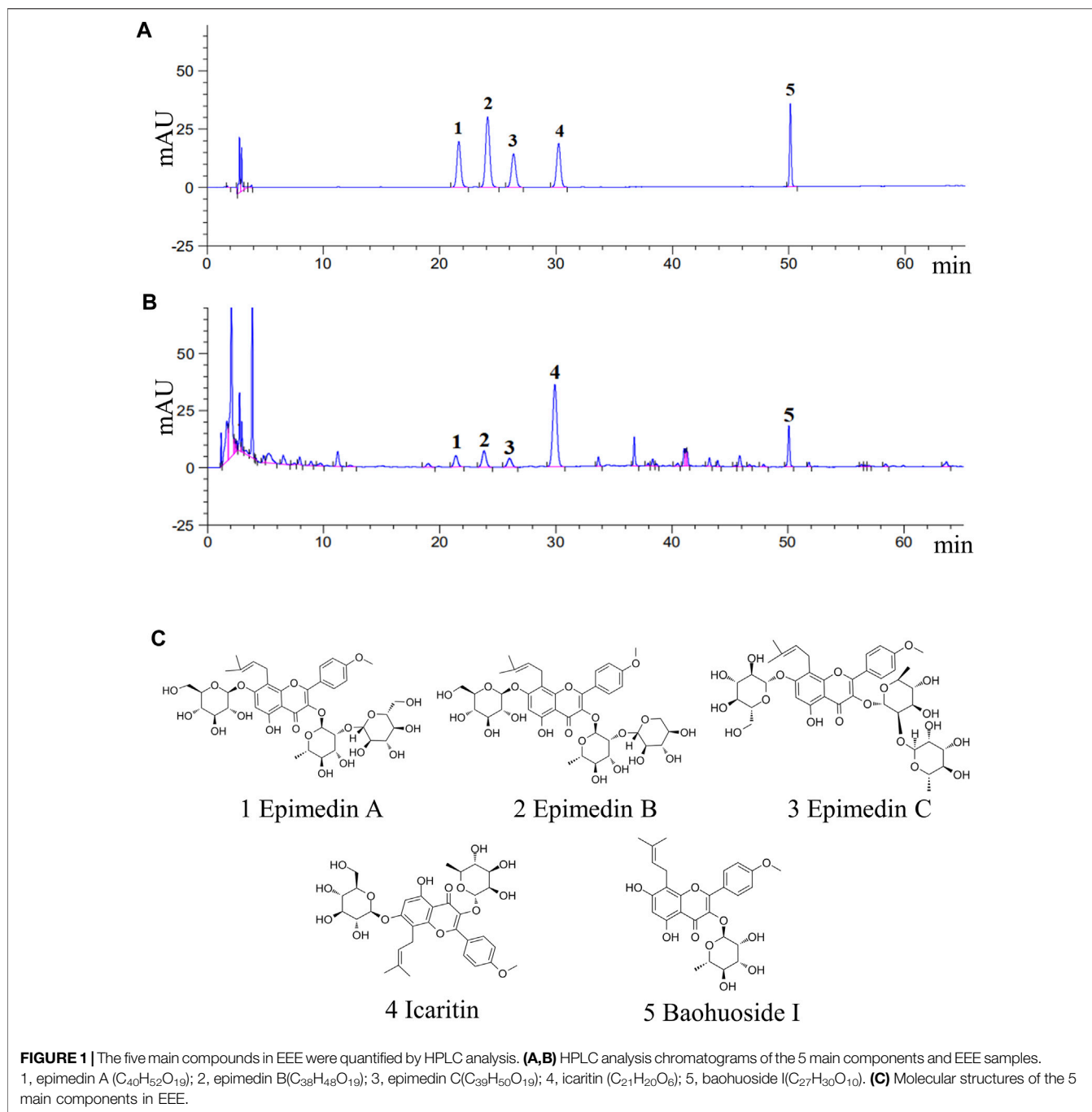
RESULTS

Major Compounds Concentrations Analysis

To ensure the reproducibility and accuracy of the experimental procedure, it is important to evaluate the quality of EEE. Five major components (epimedin A, epimedin B, epimedin C, icaritin, and baohuoside I) in EEE were selected as quality control indicators, and the concentrations of these key compounds in EEE were determined by HPLC. The concentrations of epimedin A, epimedin B, epimedin C, icaritin, and baohuoside I in EEE were 4.5, 7.3, 4.3, 31.8, 6.8 mg/g, respectively. The results are presented in **Figure 1**.

Toxic Performances of EEE-Induced Liver Injury in Rats

In this study, the body weight, organ weights, serum biochemical parameters, and liver pathology of rats after 28 days of exposure were analyzed to clarify the hepatotoxicity of EEE. Our results showed a gradual increase in body weight of rats in the control and EEE groups during the dosing period; after 28 days of exposure, the body weight

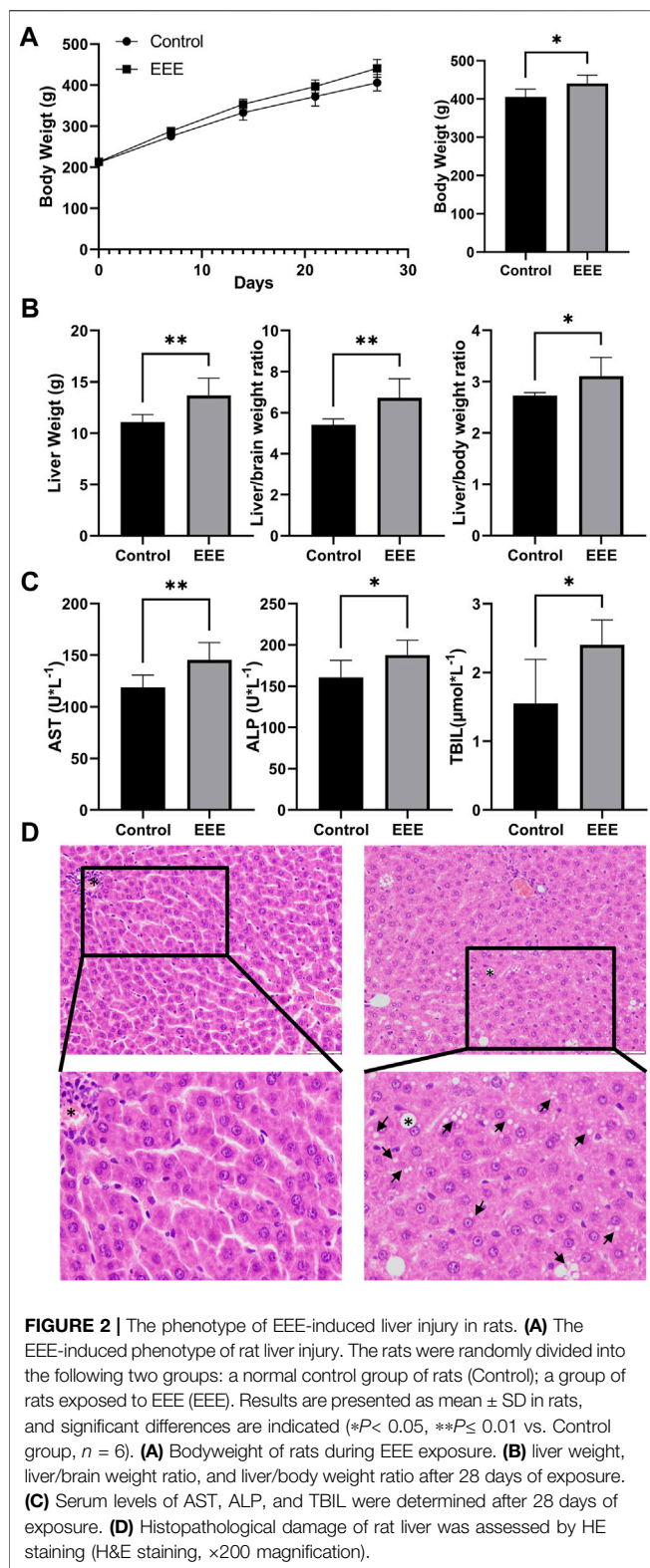


of rats in the EEE group was significantly higher than that in the control group ($p = 0.0157$) (**Figure 2A**). The liver weight, liver/brain weight ratio, and liver/body weight ratio of rats were significantly higher after EEE exposure compared with the control group ($p = 0.006, 0.008, \text{ and } 0.0322$) (**Figure 2B**). The results of serum biochemical indexes showed that AST, ALP, and TBIL were significantly higher in rats after treatment with EEE ($p = 0.01, 0.0345, \text{ and } 0.018$) (**Figure 2C**). H&E staining analysis of liver sections showed no significant histopathological damage in the control group (**Figure 2D**). In the EEE group, liver sections

showed significant histopathological changes, including visible swelling, hepatocyte steatosis, and severe cytoplasmic vacuolation (**Figure 2D**).

Liver and Serum Metabolomic Profile Analysis of EEE-Induced Liver Injury

The overall metabolic profiles of liver tissues and serum samples in the control and EEE groups were obtained by UPLC-Q-TOF/MS in positive and negative ionization modes, respectively. The



score plots of PCA analysis based on the data in positive and negative ion mode were shown in **Figures 3A–F**. The QC samples were tightly aggregated in the scoring plots for liver, serum positive ion, and negative ion modes, which indicated the

stability of the UPLC-Q-TOF/MS system throughout the analysis process and ensured the reliability and accuracy of the results. In the PCA model of liver and serum positive and negative ion assay results, a clear trend of separation was shown between the control and EEE groups (**Figures 3A,D**). This indicated that the liver and serum metabolic profiles of rats in the EEE administration group were quite different from the control group.

For further screening of differential metabolites in the liver and serum of rats after EEE exposure, the data were first analyzed by applying supervised statistical methods of OPLS-DA and S-plot. The OPLS-DA results (**Figures 3B,C,E,F**) showed significant separation between liver tissue and serum in the control and EEE groups. In the S-plots (**Figures 3B,C,E,F**), metabolites were considered to make a significant contribution to the clustering and identification between two groups when the variable VIP value ≥ 1 and $|P(\text{corr})|$ value ≥ 0.5 . Then the metabolomics data were further analyzed by using the student's t-test. Liver and serum differential metabolites that changed significantly between the control and EEE groups were screened according to VIP >1 and P < 0.05. The previously screened differential metabolites were identified by accurate mass-to-charge ratios, and the true mass error was limited to 10 ppm. The structures of the identified metabolites were analyzed and validated, and exogenous metabolites such as pharmaceuticals were removed. Finally, 78 endogenous differential metabolites were obtained in the liver, of which 40 were up-regulated and 38 down-regulated. 50 endogenous differential metabolites were obtained in serum, of which 28 were up-regulated, and 22 were down-regulated (**Figure 3G**). The m/z , retention time, and structural formulae of liver and serum differential metabolites were listed in **Supplementary Tables S1 and S2**. Cluster analysis and heatmap were performed for 78 liver differential metabolites, 50 serum differential metabolites, respectively. The results showed that the 78 liver differential metabolites and 50 serum differential metabolites could effectively distinguish the control group from the EEE group (**Figures 3I, J**).

The Metabolite Fingerprint of EEE-Induced Liver Injury

Herb-induced liver injury is insidious, so screening for appropriate serum metabolic fingerprints can help establish an early warning method to avoid liver injury. It was found that 14 differential metabolites were significantly different in both liver and serum after EEE exposure (**Figure 3H**). Among the 14 shared differential metabolites, 12 showed consistent changes in liver and serum (**Figures 4A,B**). Among them, glutathione (GSH), sphingomyelin, cholic acid, deoxycholic acid, N-acetylhistamine, and phenylacetylglycine were significantly decreased in liver and serum after EEE exposure. Flavin mononucleotide (FMN), L-tryptophan, fumaric acid, N-acetyloronithine, hippuric acid, and lumichrome were significantly increased in liver and serum after EEE exposure. ROC curves were used to analyze the predictive performance of 14 differential metabolites for liver injury, and the top 4 differential metabolites with AUC values in liver and serum were selected to plot ROC curves (**Figures 4C–F**).

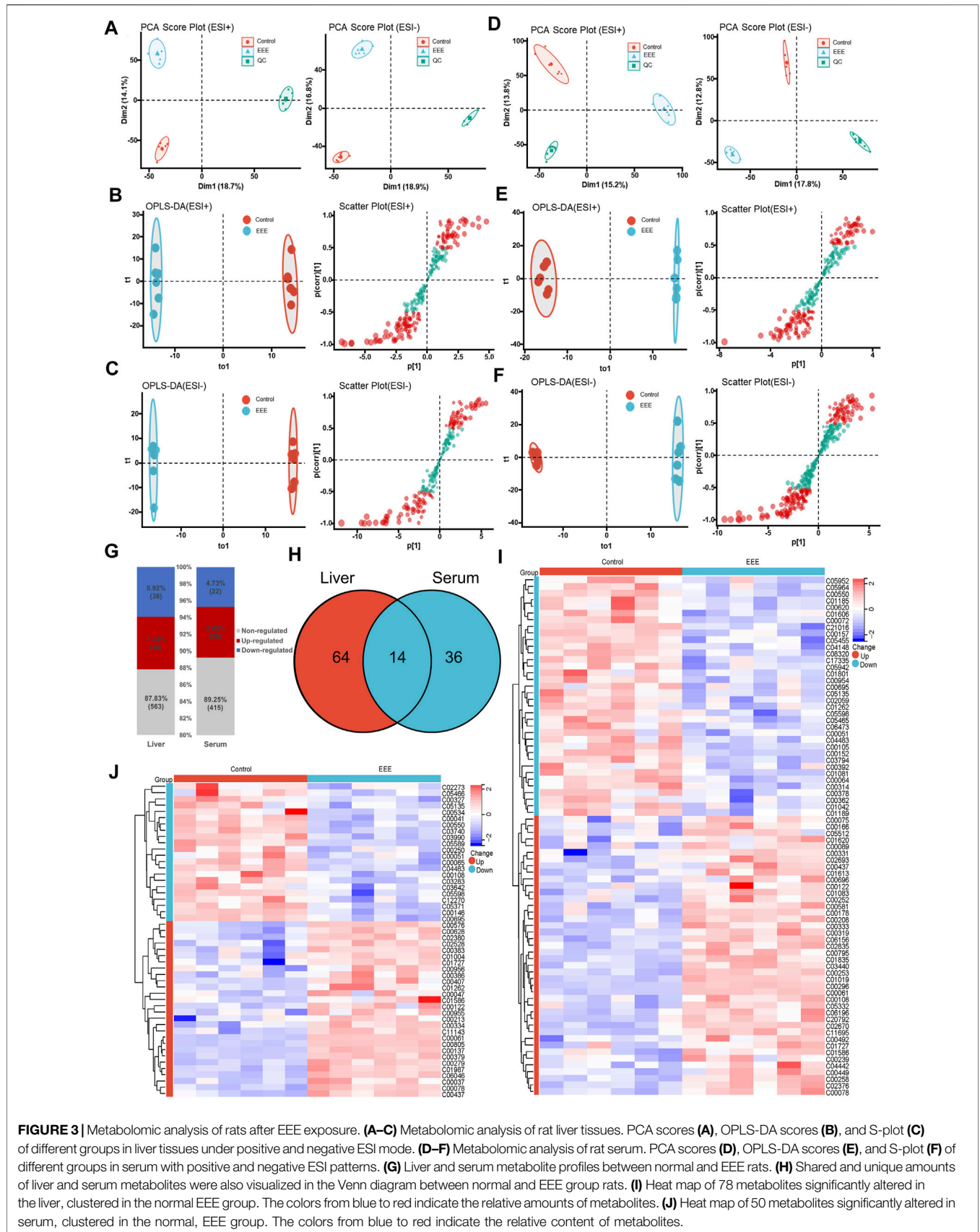
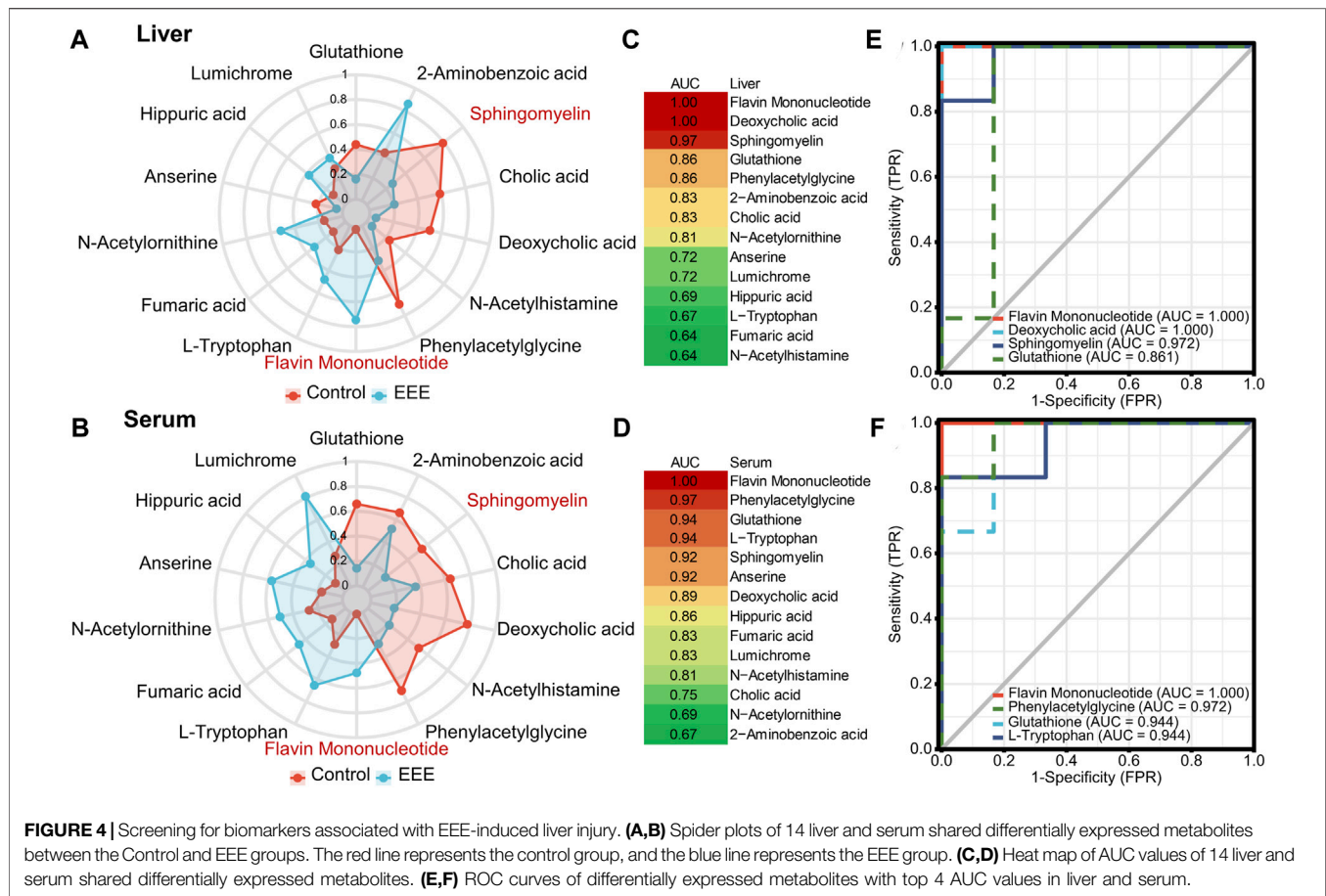


FIGURE 3 | Metabolomic analysis of rats after EEE exposure. **(A–C)** Metabolomic analysis of rat liver tissues. PCA scores **(A)**, OPLS-DA scores **(B)**, and S-plot **(C)** of different groups in liver tissues under positive and negative ESI mode. **(D–F)** Metabolomic analysis of rat serum. PCA scores **(D)**, OPLS-DA scores **(E)**, and S-plot **(F)** of different groups in serum with positive and negative ESI patterns. **(G)** Liver and serum metabolite profiles between normal and EEE rats. **(H)** Shared and unique amounts of liver and serum metabolites were also visualized in the Venn diagram between normal and EEE group rats. **(I)** Heat map of 78 metabolites significantly altered in the liver, clustered in the normal EEE group. The colors from blue to red indicate the relative amounts of metabolites. **(J)** Heat map of 50 metabolites significantly altered in the serum, clustered in the normal, EEE group. The colors from blue to red indicate the relative content of metabolites.



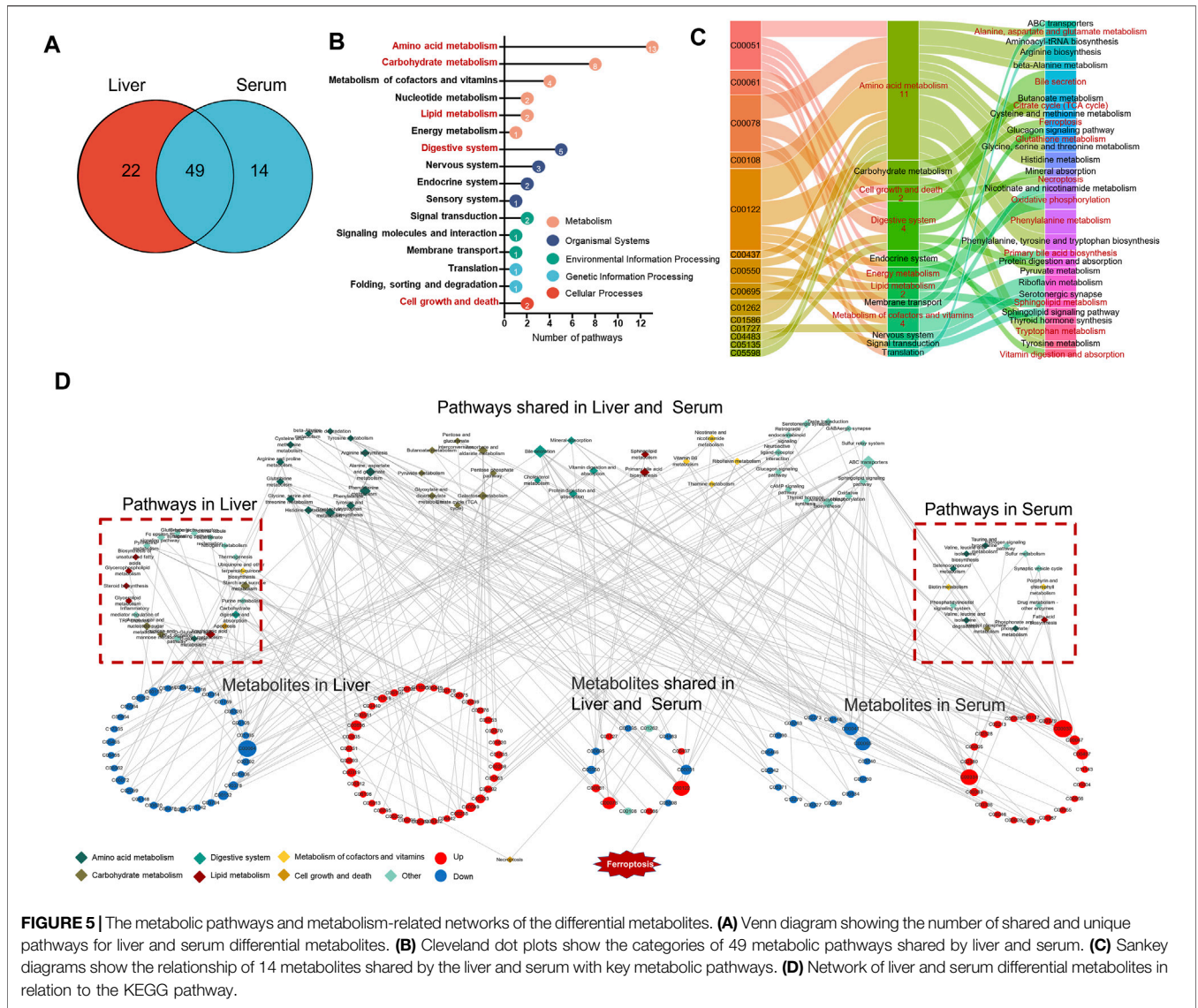
In the liver, three metabolites' AUC values > 0.9, including FMN, deoxycholic acid, and sphingomyelin. In serum, six metabolites' AUC values > 0.9, including FMN, phenylacetylglutamine, GSH, L-tryptophan, sphingomyelin, and anserine. Among them, the AUC values of FMN and sphingomyelin were greater than 0.9 in both liver and serum, which could be used as potential biomarkers of EEE hepatotoxicity.

Pathway Enrichment and Mechanisms Analysis

To further analyze the effect of EEE exposure on metabolic pathways, the obtained differential metabolites in liver and serum were submitted into MetaboAnalyst 5.0 for KEGG pathway analysis, and the results revealed that the differential metabolites in liver and serum were respectively enriched to 71 and 64 pathways, of which 49 pathways were shared (**Figure 5A**). According to the KEGG pathway classification, 49 shared pathways are mainly involved in amino acid metabolism, lipid metabolism, digestive system, carbohydrate metabolism, metabolism of cofactors and vitamins, cell growth and death, etc. (**Figure 5B**). The disturbances of alanine, aspartate and glutamate metabolism, phenylalanine metabolism, arginine biosynthesis, tryptophan metabolism, and glutathione metabolism were observed in amino acid metabolism,

disturbances in primary bile acid biosynthesis and sphingolipid metabolism were observed in lipid metabolism, and the disturbances in tricarboxylic citrate cycle, pentose phosphate pathway, and pyruvate metabolism were observed in carbohydrate metabolism. For the digestive system, disturbances in bile secretion, cholesterol metabolism, and other pathways were observed. In addition to the disruptions of thiamine metabolism, riboflavin metabolism, vitamin B6 metabolism, and ferroptosis and necroptosis pathways were observed (**Figure 5C**).

The KEGG enrichment results were imported into Cytoscape software to construct the KEGG pathways-metabolites network (**Figure 5D**), it was found that EEE could broadly affect amino acid and lipid metabolism in rats, mainly including primary bile acid biosynthesis, sphingolipid metabolism, bile secretion, cholesterol metabolism, and glutathione metabolism. These pathways are mainly involved in the metabolism of glutathione and the biosynthesis of unsaturated fatty acids. Among these pathways, studies have shown that glutathione metabolism, cholesterol metabolism, and sphingolipid metabolism are closely related to ferroptosis (Agmon and Stockwell, 2017; Stockwell et al., 2020; Liu et al., 2021). Also, the key differential metabolites of GSH, FMN, fumaric acid, etc. in these pathways have important roles in ferroptosis (Ursini and Maiorino, 2020; Wang H et al., 2020; Vabulas, 2021).



Combining the above metabolic pathway analysis, the hypothesis was proposed that EEE caused liver injury by inducing ferroptosis.

EEE-Induced Liver Injury Associated With Ferroptosis

To verify whether EEE causes liver injury by inducing ferroptosis in the liver of rats, the typical indicators related to ferroptosis were examined, including the lipid peroxidation marker (MDA), intracellular major antioxidant activity enzyme (SOD), ferroptosis inhibitory protein (GPX4), System x_c^- , ferroptosis-promoting protein (ACSL4). The results showed that EEE exposure could significantly increase MDA content and significantly lower SOD activity in rat liver ($P = 0.0147, 0.0084$) (Figures 6A,B). In addition, the results of the Western blot assay showed that EEE exposure significantly decreased the protein expression of glutathione peroxidase 4 (GPX4), System

x_c^- , while the expression of ACSL4 protein significantly increased ($P = 0.0066, 0.0155, 0.0071$) (Figures 6C-F). Taken together, these results supported that liver injury in rats after EEE exposure could be strongly associated with ferroptosis.

DISCUSSION

The factors contributing to liver toxicity with herbal medicines are complex, and studying their mechanisms is a great challenge. Liver plays a crucial role in the metabolism, detoxification, and excretion of exogenous chemicals (Sun et al., 2021). When herbal medicines enter the body, they undergo metabolic reactions, and endogenous small molecules change over time as they are metabolized, and these changes in endogenous small molecules may induce liver injury (Liu et al., 2016). Metabolomics is used to characterize changes in the organism in response to external factors by detecting small molecules at the most downstream level

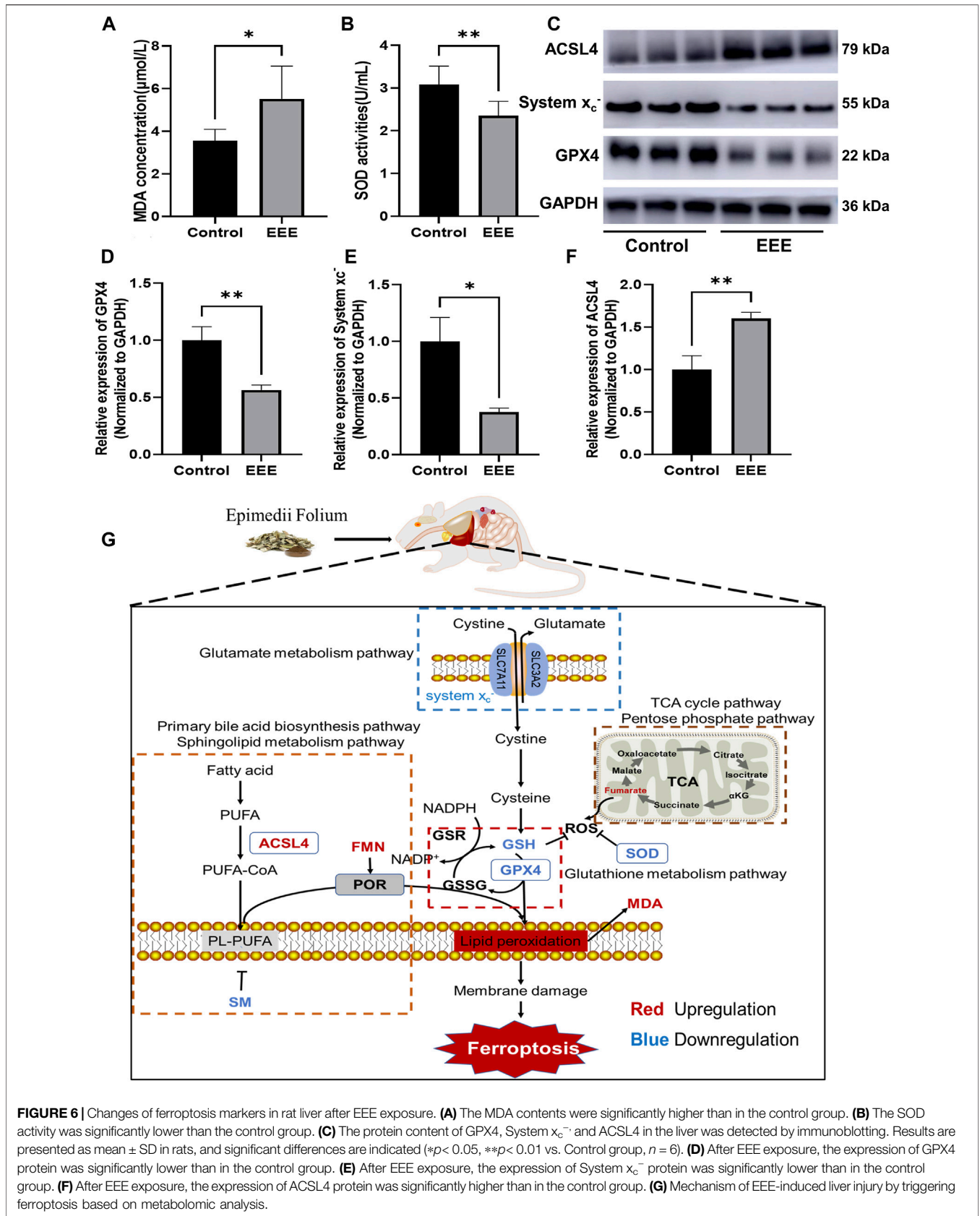


FIGURE 6 | Changes of ferroptosis markers in rat liver after EEE exposure. **(A)** The MDA contents were significantly higher than in the control group. **(B)** The SOD activity was significantly lower than the control group. **(C)** The protein content of GPX4, System x_c^- and ACSL4 in the liver was detected by immunoblotting. Results are presented as mean \pm SD in rats, and significant differences are indicated (* $p < 0.05$, ** $p < 0.01$ vs. Control group, $n = 6$). **(D)** After EEE exposure, the expression of GPX4 protein was significantly lower than in the control group. **(E)** After EEE exposure, the expression of System x_c^- protein was significantly lower than in the control group. **(F)** After EEE exposure, the expression of ACSL4 protein was significantly higher than in the control group. **(G)** Mechanism of EEE-induced liver injury by triggering ferroptosis based on metabolomic analysis.

of the system biology (Cuykx et al., 2018). This makes metabolomics fingerprinting very sensitive, and even small external factors may induce changes. Metabolomics allows systematic filtering of the metabolic change patterns of the body through the analysis of endogenous metabolites (Wang et al., 2011). And metabolomics helps to identify potential biomarkers and disordered metabolic pathways by comparing metabolic profiles in normal and toxic states, thus elucidating possible mechanisms (Chen et al., 2020). In this study, the hepatotoxicity of EEE in rats was evaluated, and the relevant mechanisms were explored.

Our results showed that the liver weight, liver/body weight ratio, and liver/brain weight ratio of EEE-exposed rats were significantly higher than those of the control group (Figures 2A,B). This demonstrated the toxic effects of EEE on the liver. Serum biochemical parameters are the most commonly used markers of liver function (Green and Flamm, 2002). In our experiments, AST, ALP, and TBIL in the serum of rats exposed to EEE were significantly altered compared with control rats (Figure 2C). Pathology of the liver by microscopy revealed severe cytoplasmic vacuolation in liver cells of rats in the EEE group. Organ weight is one of the most sensitive toxicity indicators, and changes are often earlier or more severe than changes in histopathology or serum indicators (Piao et al., 2013); our results showed that the differences in the indicators such as liver weight, liver/body weight ratio, and liver/brain weight ratio of rats were more obvious than serum biochemical indicators such as AST, ALP, this suggested that the effects of EEE on the liver itself predate the changes in blood biochemistry. These results suggested that EEE might have caused significant damage to the rat liver; how EEE induces these pathological changes requires further investigation.

A metabolomic approach was applied to explore the mechanism of EEE-induced liver injury. The results revealed that EEE exposure led to extensive differences in the metabolism of serum and liver in rats. In-depth analysis revealed that 14 identical endogenous metabolites in serum and liver were significantly different from the normal group after EEE exposure and could serve as metabolic fingerprints for EEE-induced liver injury. Among them, FMN and sphingomyelin had AUC values greater than 0.9 in both liver and serum by ROC analysis and could be used to predict hepatotoxicity of EEE. And the subsequent analysis showed that FMN and sphingomyelin had an important role in the mechanism of EEE-induced liver injury.

The KEGG pathway enrichment analysis was performed on differential metabolites to deeply analyze the mechanism of liver injury caused by EEE. The enrichment results showed that EEE exposure had a great effect on amino acid metabolism, lipid metabolism pathways, especially on primary bile acid biosynthesis, sphingolipid metabolism, bile secretion, cholesterol metabolism, glutathione metabolism, and other pathways related to glutathione metabolism and unsaturated fatty acid biosynthesis metabolism have greater interference (Figures 5A–C). Extensive studies have shown that unsaturated fatty acid peroxidation due to abnormal glutathione metabolism is one of the typical features of

ferroptosis (Xie et al., 2016; Doll et al., 2019; Li et al., 2020) (Figure 5D). Ferroptosis is a new type of cell death discovered in recent years, and the process of cell death is usually accompanied by massive iron accumulation and lipid peroxidation (Chen et al., 2021). Increased lipid peroxide content is an important marker for the development of ferroptosis. MDA is one of the degradation products of polyunsaturated fatty acid peroxides, and MDA increases significantly when ferroptosis occurs (Tang et al., 2021). Superoxide dismutase (SOD) is widely found in human tissues and is an important antioxidant that plays an important role in maintaining the redox balance of cells (Rosa et al., 2021). Our previous study found that EEE significantly enhanced reactive oxygen species (ROS) levels, decreased GSH levels, and promoted MDA production in HL7702 and HepG2 cells *in vitro* (Zhang L et al., 2020). Based on these results, we hypothesize that ferroptosis may be the key to EEE-induced liver injury.

The related markers were analyzed to confirm the conjecture that EEE causes ferroptosis; the results of metabolomic showed that GSH in the liver and serum of rats was significantly reduced after EEE exposure (Figures 4A,B). Meanwhile, the SOD activity in liver tissues was significantly decreased, and the level of MDA was significantly increased (Figures 6A,B). Among them, the changes in GSH and MDA were consistent with the results of our previously published *in vitro* experiments. In addition, the metabolomic analysis revealed significantly higher levels of fumaric acid in liver tissue and serum of rats in the EEE group (Figures 4A,B). It has been found that glutathione succinate (GSF), the covalently bound product of fumaric acid and glutathione, is a substrate for glutathione reductase and can enhance ROS production by consuming NADPH (Sullivan et al., 2013). This finding is consistent with the *in vitro* results that ROS levels were significantly increased in HL7702 and HepG2 cells after EEE incubation. In conclusion, the above results demonstrated that EEE induced ferroptosis in rat liver by disrupting redox balance.

Ferroptosis initiation and execution are tightly controlled by iron, lipid, amino acid, and glutathione metabolism; the results of metabolomic showed that amino acid and glutathione metabolic pathways were extensively affected in rat liver after EEE exposure (Figure 5B), the cystine/glutamate transporter (System x_c^-) is involved in this procedure and plays an important part in the process (Koppula et al., 2018). The System x_c^- is an amino acid antiporter, a transmembrane structure formed by light solute carrier family 7 member 11 and Solute Carrier Family 3 Member 2 (Liu et al., 2020). The System x_c^- is primarily responsible for pumping intracellular glutamate out of the cell in exchange for extracellular cysteine (Koppula et al., 2021). Cystine entering the cell is converted to cysteine, which is then combined with glutamate and glycine to synthesize the endogenous antioxidant GSH (Lu, 2009), GSH is a tripeptide antioxidant and a cofactor of selenium-dependent GPX4 in reducing lipid peroxidation, reduced GSH synthesis can indirectly inactivate GPX4, lead to the bioaccumulation of intracellular ROS and cause lipid peroxidation (Dixon et al., 2012). GPX4, a member of the GPX family, is the only enzyme, which reduces phospholipid hydrogen peroxide and plays an essential role in maintaining

redox homeostasis in cells, GPX4 limits the propagation of lipid peroxidation in membranes by reducing toxic lipid peroxides (L-OOH) to non-toxic lipid alcohols (L-OH), which in turn prevents ferroptosis (Forcina and Dixon, 2019). Thus, ferroptosis is irreversible when oxidative damage leads to a large production of lipid peroxides or when excessive depletion of GSH leads to a decrease in GPX4 activity (Yang and Stockwell, 2016). Recent studies have shown that inhibition of the System x_c^- , which reduces the uptake of cystine, impairs the antioxidant defense system of cells and eventually leads to ferroptosis (Dixon et al., 2014). It was also found that overexpression of GPX4 in cells caused resistance to ferroptosis, while knockdown of GPX4 promoted ferroptosis (Bersuker et al., 2019). Therefore, with reduced GPX4, System x_c^- expression is a key marker of ferroptosis. In our experiments, the expression of System x_c^- and GPX4 in rat liver was significantly reduced after EEE exposure (Figures 6D,E), which is one of the pieces of evidence confirming that EEE might induce ferroptosis. Iron-catalyzed excessive peroxidation of phospholipids (PLs) containing polyunsaturated fatty acids (PUFAs) is a major feature of ferroptosis, and these phospholipids are abundant in mammalian cell membranes (Tang et al., 2021).

The results of metabolomic showed that fatty acid metabolism pathways such as the Primary bile acid biosynthesis pathway and sphingolipid metabolism pathway in rat livers were extensively affected after EEE exposure (Figure 5B, Figure 6G). The study revealed through lipidomic analysis that Acyl-CoA Synthetase Long Chain Family Member 4 (ACSL4) could have an essential role in ferroptosis by regulating the metabolism of lipid components (Doll et al., 2017). Several studies have identified ACSL4 as a key factor in determining ferroptosis sensitivity (Yuan et al., 2016; Doll et al., 2017; Kagan et al., 2017). A significant increase in ACSL4 expression in rat liver tissue after exposure to EEE was observed (Figures 6C,F). Therefore, based on the above results, we infer that EEE may induce hepatic lipid metabolism disturbance and promote ferroptosis by upregulating ACSL4.

In addition, interestingly, FMN, sphingomyelin, which had AUC values greater than 0.9 in both liver and serum, also had an important role in ferroptosis. Among them, FMN is a biomolecule produced by riboflavin (vitamin B2) through riboflavin kinase, which is an auxiliary group of various oxidoreductases (such as NADH dehydrogenase) (Akasov et al., 2019). FMN is a more potent oxidant than Nicotinamide adenine dinucleotide (NAD) and enhances the ability of cytochrome P450 oxidoreductase (POR) to auto-oxidize and produce ROS, and promotes PUFAs peroxidation to induce ferroptosis (Esteves et al., 2020; Yan et al., 2021). Sphingolipids are significant components of animal plasma membranes; some studies have found that it may act as a “biophysical antioxidant” by changing the oxidation rate of PUFA, limiting the propagation of the lipid peroxidation process, and thereby reducing ferroptosis (Coliva et al., 2020; Aldrovandi et al., 2021). Our experiments revealed that the content of FMN in the liver and serum was significantly increased, and the content of sphingomyelin was significantly

decreased after EEE exposure (Figures 4A,B). These also indicated that EEE exposure resulted in severe redox derangements in rat liver, leading to the development of lipid peroxidation, which in turn caused ferroptosis in hepatocytes.

Some researchers have found that GPX4 and GSH, which have important regulatory roles in ferroptosis, may have inhibitory effects on NLRP3 inflammasome activation (Wang et al., 2019; Zhang et al., 2021). In our study, it was also found that GPX4 and GSH decreased after EEE administration, which could not only induce ferroptosis in liver cells to produce direct toxicity, but also lead to non-specific liver injury by activating the NLRP3 inflammasome. According to literature reports, not only EEE can cause direct liver injury, but its main components such as icaricide I and icaricide II can also induce idiosyncratic liver injury (IDILI) by activating the NLRP3 inflammasome (Wang Z et al., 2020; Gao et al., 2021). In addition, in the KEGG pathway analysis, we found that metabolic disturbance caused by EEE might also cause necroptosis in hepatocytes. Necroptosis is a way of programmed cell death mediated by inflammation (Dhuriya and Sharma, 2018). NLRP3 inflammasome activation often leads to necroptosis in cells (Huang et al., 2021). In addition, studies have found that GPX4 is not only an inhibitor of ferroptosis, but also plays an important role in inhibiting necroptosis (Canli et al., 2016). At the same time, some studies have found that the redox homeostasis of cells also plays an important role in necroptosis (Florea et al., 2019; Zhang Y et al., 2020; Li et al., 2021). Decreased GSH and SOD levels lead to increased oxidative stress in cells, which can induce necroptosis in cells (Xie et al., 2015). Taken together, EEE exposure caused a severe imbalance in redox homeostasis in the rat organism, induced ferroptosis in hepatocytes, and activated inflammatory pathways promoting necroptosis. As for the relationship between EEE and IDILI, we expected to have some new findings in further research. In combination, we found that the liver injury caused by EEE exposure might be related to the extensive disruption of amino acid metabolism, glutathione metabolism, and lipid metabolism in rat liver, and the regulation of the expression of key ferroptosis proteins such as GPX4, System x_c^- , and ACSL4, resulting in the decrease of antioxidant active substances such as GSH, sphingomyelin and SOD, and the increase of pro-oxidant active substances such as FMN and ROS, which disrupt the redox balance in the liver and promote lipid peroxidation (increased MDA content), causing ferroptosis (Figure 6G).

CONCLUSION

In conclusion, our study confirmed that EEE could induce liver injury in rats, and its hepatotoxicity mechanism was related to the induction of ferroptosis in hepatocytes. During the performance of metabolic profiling of rat liver and serum, we found the metabolic difference and screened two differential metabolites (FMN, SM) shared by liver and serum as potential biomarkers for EEE-induced liver injury (ROC AUC >0.9). By analyzing the differential metabolites and enrichment pathways, the results suggested that EEE might induce liver injury by

disrupting the redox homeostasis of rat liver tissue inducing ferroptosis. This finding was confirmed by the expression of ferroptosis marker proteins GPX4, System x_c^- , ACSL4, as well as SOD activity and MDA content in the liver. These results provided a theoretical basis for further research on the mechanism of EEE-induced liver injury. However, there were some limitations in this study. The current experimental results did not fully uncover the mechanism of *Epimedium koreanum* Nakai hepatotoxicity, and the main components responsible for hepatotoxicity had not been clarified, which needed further exploration and research.

DATA AVAILABILITY STATEMENT

The original contributions presented in the study are included in the article/**Supplementary Material**; further inquiries can be directed to the corresponding authors.

ETHICS STATEMENT

The animal study was reviewed and approved by the Center for Experimental Animal Welfare and Ethics of Beijing University of Traditional Chinese Medicine.

REFERENCES

- Agmon, E., and Stockwell, B. R. (2017). Lipid Homeostasis and Regulated Cell Death. *Curr. Opin. Chem. Biol.* 39, 83–89. doi:10.1016/j.cbpa.2017.06.002
- Akasov, R. A., Sholina, N. V., Khochenkov, D. A., Alova, A. V., Gorelkin, P. V., Erofeev, A. S., et al. (2019). Photodynamic Therapy of Melanoma by Blue-Light Photoactivation of Flavin Mononucleotide. *Sci. Rep.* 9, 9679. doi:10.1038/s41598-019-46115-w
- Aldrovandi, M., Fedorova, M., and Conrad, M. (2021). Juggling with Lipids, a Game of Russian Roulette. *Trends Endocrinol. Metab.* 32, 463–473. doi:10.1016/j.tem.2021.04.012
- Bersuker, K., Hendricks, J. M., Li, Z., Magtanong, L., Ford, B., Tang, P. H., et al. (2019). The CoQ Oxidoreductase FSP1 Acts Parallel to GPX4 to Inhibit Ferroptosis. *Nature* 575, 688–692. doi:10.1038/s41586-019-1705-2
- Brown, A. C. (2017). Liver Toxicity Related to Herbs and Dietary Supplements: Online Table of Case Reports. Part 2 of 5 Series. *Food Chem. Toxicol.* 107, 472–501. doi:10.1016/j.fct.2016.07.001
- Canli, Ö., Alankuş, Y. B., Grootjans, S., Vegi, N., Hültner, L., Hoppe, P. S., et al. (2016). Glutathione Peroxidase 4 Prevents Necroptosis in Mouse Erythroid Precursors. *Blood* 127, 139–148. doi:10.1182/blood-2015-06-654194
- Chen, J. Q., Chen, Y. Y., Tao, H. J., Pu, Z. J., Shi, X. Q., Zhang, J., et al. (2020). An Integrated Metabolomics Strategy to Reveal Dose-Effect Relationship and Therapeutic Mechanisms of Different Efficacy of Rhubarb in Constipation Rats. *J. Pharm. Biomed. Anal.* 177, 112837. doi:10.1016/j.jpba.2019.112837
- Chen, X., Yu, C., Kang, R., Kroemer, G., and Tang, D. (2021). Cellular Degradation Systems in Ferroptosis. *Cell Death Differ.* 28, 1135–1148. doi:10.1038/s41418-020-00728-1
- Cheng, Y., Liu, Y., Wang, H., Li, J., Ren, J., Zhu, L., et al. (2013). A 26-week Repeated Dose Toxicity Study of Xian-Ling-Gu-Bao in Sprague-Dawley Rats. *J. Ethnopharmacol.* 145, 85–93. doi:10.1016/j.jep.2012.09.055
- Chinese Pharmacopoeia Commission (2020). *Pharmacopoeia of the People's Republic of China*. 2020 edition. Beijing, China: China Medical Science and Technology Press.
- Coliva, G., Lange, M., Colombo, S., Chervet, J. P., Domingues, M. R., and Fedorova, M. (2020). Sphingomyelins Prevent Propagation of Lipid Peroxidation-LC-MS/

AUTHOR CONTRIBUTIONS

LZ, TW designed and supervised the research. PL, CC participated in the animal experiments. CC, ZG, QK, XL, QM, and YH took part in collecting tissue samples at the end of the experiment. JZ performed the pathological data analysis. LZ, PL performed the data analysis for metabolomics. LZ, PL prepared the manuscript draft. LZ and TW revised the manuscript and provided extensive discussions. All authors participated in the discussions and editing of the manuscript.

FUNDING

This study was supported by the National Natural Science Funds of China (Grant No. 82004053) and the New Teacher Initial Fund Project of the Beijing University of Chinese Medicine (Grant No. 2020-JYB-XJSJJ-020).

SUPPLEMENTARY MATERIAL

The Supplementary Material for this article can be found online at: <https://www.frontiersin.org/articles/10.3389/fphar.2022.934057/full#supplementary-material>

- MS Evaluation of Inhibition Mechanisms. *Molecules* 25, 1925. doi:10.3390/molecules25081925
- Cuykx, M., Rodrigues, R. M., Laukens, K., Vanhaecke, T., and Covaci, A. (2018). *In Vitro* Assessment of Hepatotoxicity by Metabolomics: a Review. *Arch. Toxicol.* 92, 3007–3029. doi:10.1007/s00204-018-2286-9
- Dhuriya, Y. K., and Sharma, D. (2018). Necroptosis: a Regulated Inflammatory Mode of Cell Death. *J. Neuroinflammation* 15, 199. doi:10.1186/s12974-018-1235-0
- Dixon, S. J., Lemberg, K. M., Lamprecht, M. R., Skouta, R., Zaitsev, E. M., Gleason, C. E., et al. (2012). Ferroptosis: an Iron-dependent Form of Nonapoptotic Cell Death. *Cell* 149, 1060–1072. doi:10.1016/j.cell.2012.03.042
- Dixon, S. J., Patel, D. N., Welsch, M., Skouta, R., Lee, E. D., Hayano, M., et al. (2014). Pharmacological Inhibition of Cystine-Glutamate Exchange Induces Endoplasmic Reticulum Stress and Ferroptosis. *Elife* 3, e02523. doi:10.7554/eLife.02523
- Doll, S., Proneth, B., Tyurina, Y. Y., Panzilius, E., Kobayashi, S., Ingold, I., et al. (2017). ACSL4 Dictates Ferroptosis Sensitivity by Shaping Cellular Lipid Composition. *Nat. Chem. Biol.* 13, 91–98. doi:10.1038/nchembio.2239
- Doll, S., Freitas, F. P., Shah, R., Aldrovandi, M., da Silva, M. C., Ingold, I., et al. (2019). FSP1 Is a Glutathione-independent Ferroptosis Suppressor. *Nature* 575, 693–698. doi:10.1038/s41586-019-1707-0
- Duan, L., Guo, L., Wang, L., Yin, Q., Zhang, C. M., Zheng, Y. G., et al. (2018). Application of Metabolomics in Toxicity Evaluation of Traditional Chinese Medicines. *Chin. Med.* 13, 60. doi:10.1186/s13020-018-0218-5
- Esteves, F., Campelo, D., Gomes, B. C., Urban, P., Bozonnet, S., Lautier, T., et al. (2020). The Role of the FMN-Domain of Human Cytochrome P450 Oxidoreductase in its Promiscuous Interactions with Structurally Diverse Redox Partners. *Front. Pharmacol.* 11, 299. doi:10.3389/fphar.2020.00299
- Florean, C., Song, S., Dicato, M., and Diederich, M. (2019). Redox Biology of Regulated Cell Death in Cancer: A Focus on Necroptosis and Ferroptosis. *Free Radic. Biol. Med.* 134, 177–189. doi:10.1016/j.freeradbiomed.2019.01.008
- Forcina, G. C., and Dixon, S. J. (2019). GPX4 at the Crossroads of Lipid Homeostasis and Ferroptosis. *Proteomics* 19, e1800311. doi:10.1002/pmic.201800311
- Gao, Y., Xu, G., Ma, L., Shi, W., Wang, Z., Zhan, X., et al. (2021). Icariside I Specifically Facilitates ATP or Nigericin-Induced NLRP3 Inflammasome

- Activation and Causes Idiosyncratic Hepatotoxicity. *Cell Commun. Signal* 19, 13. doi:10.1186/s12964-020-00647-1
- García-Cortés, M., Robles-Díaz, M., Ortega-Alonso, A., Medina-Caliz, I., and Andrade, R. (2016). Hepatotoxicity by Dietary Supplements: A Tabular Listing and Clinical Characteristics. *Int. J. Mol. Sci.* 17, 537. doi:10.3390/ijms17040537
- Gika, H., Virgiliou, C., Theodoridis, G., Plumb, R. S., and Wilson, I. D. (2019). Untargeted LC/MS-based Metabolic Phenotyping (Metabonomics/metabolomics): The State of the Art. *J. Chromatogr. B Anal. Technol. Biomed. Life Sci.* 1117, 136–147. doi:10.1016/j.jchromb.2019.04.009
- Gong, Z. G., Hu, J., Wu, X., and Xu, Y. J. (2017). The Recent Developments in Sample Preparation for Mass Spectrometry-Based Metabolomics. *Crit. Rev. Anal. Chem.* 47, 325–331. doi:10.1080/10408347.2017.1289836
- Green, R. M., and Flamm, S. (2002). AGA Technical Review on the Evaluation of Liver Chemistry Tests. *Gastroenterology* 123, 1367–1384. doi:10.1053/gast.2002.36061
- Huang, Y., Xu, W., and Zhou, R. (2021). NLRP3 Inflammasome Activation and Cell Death. *Cell Mol. Immunol.* 18, 2114–2127. doi:10.1038/s41423-021-00740-6
- Iorga, A., Dara, L., and Kaplowitz, N. (2017). Drug-Induced Liver Injury: Cascade of Events Leading to Cell Death, Apoptosis or Necrosis. *Int. J. Mol. Sci.* 18, 1018. doi:10.3390/ijms18051018
- Kagan, V. E., Mao, G., Qu, F., Angeli, J. P., Doll, S., Croix, C. S., et al. (2017). Oxidized Arachidonic and Adrenic PEs Navigate Cells to Ferroptosis. *Nat. Chem. Biol.* 13, 81–90. doi:10.1038/nchembio.2238
- Koppula, P., Zhang, Y., Zhuang, L., and Gan, B. (2018). Amino Acid Transporter SLC7A11/xCT at the Crossroads of Regulating Redox Homeostasis and Nutrient Dependency of Cancer. *Cancer Commun. (Lond)* 38, 12. doi:10.1186/s40880-018-0288-x
- Koppula, P., Zhuang, L., and Gan, B. (2021). Cystine Transporter SLC7A11/xCT in Cancer: Ferroptosis, Nutrient Dependency, and Cancer Therapy. *Protein Cell* 12, 599–620. doi:10.1007/s13238-020-00789-5
- Li, J., Cao, F., Yin, H. L., Huang, Z. J., Lin, Z. T., Mao, N., et al. (2020). Ferroptosis: Past, Present, and Future. *Cell Death Dis.* 11, 88. doi:10.1038/s41419-020-2298-2
- Li, T., Zhang, J., Wang, P.-J., Zhang, Z.-W., and Huang, J.-Q. (2021). Selenoproteins Protect against Avian Liver Necrosis by Metabolizing Peroxides and Regulating Receptor Interacting Serine Threonine Kinase 1/ Receptor Interacting Serine Threonine Kinase 3/Mixed Lineage Kinase Domain-like and Mitogen-Activated Protein Kinase Signaling. *Front. Physiol.* 12, 696256. doi:10.3389/fphys.2021.696256
- Liu, C., Fan, H., Li, Y., and Xiao, X. (2016). Research Advances on Hepatotoxicity of Herbal Medicines in China. *Biomed. Res. Int.* 2016, 7150391. doi:10.1155/2016/7150391
- Liu, J., Xia, X., and Huang, P. (2020). xCT: A Critical Molecule that Links Cancer Metabolism to Redox Signaling. *Mol. Ther.* 28, 2358–2366. doi:10.1016/j.yimthe.2020.08.021
- Liu, W., Chakraborty, B., Safi, R., Kazmin, D., Chang, C. Y., and McDonnell, D. P. (2021). Dysregulated Cholesterol Homeostasis Results in Resistance to Ferroptosis Increasing Tumorigenicity and Metastasis in Cancer. *Nat. Commun.* 12, 5103. doi:10.1038/s41467-021-25354-4
- Lu, S. C. (2009). Regulation of Glutathione Synthesis. *Mol. Asp. Med.* 30, 42–59. doi:10.1016/j.mam.2008.05.005
- Luo, Y., Gao, F., Chang, R., Zhang, X., Zhong, J., Wen, J., et al. (2021). Metabolomics Based Comprehensive Investigation of Gardeniae Fructus Induced Hepatotoxicity. *Food Chem. Toxicol.* 153, 112250. doi:10.1016/j.fct.2021.112250
- Ma, H., He, X., Yang, Y., Li, M., Hao, D., and Jia, Z. (2011). The Genus Epimedium: an Ethnopharmacological and Phytochemical Review. *J. Ethnopharmacol.* 134, 519–541. doi:10.1016/j.jep.2011.01.001
- Navarro, V. J., Khan, I., Björnsson, E., Seeff, L. B., Serrano, J., and Hoofnagle, J. H. (2017). Liver Injury from Herbal and Dietary Supplements. *Hepatology* 65, 363–373. doi:10.1002/hep.28813
- Phapale, P. (2021). Pharmacometabolomics Opportunities in Drug Development and Clinical Research. *Anal. Sci. Adv.* 2, 611–616. doi:10.1002/ansa.202000178
- Piao, Y., Liu, Y., and Xie, X. (2013). Change Trends of Organ Weight Background Data in Sprague Dawley Rats at Different Ages. *J. Toxicol. Pathol.* 26, 29–34. doi:10.1293/tox.26.29
- Rosa, A. C., Bruni, N., Meineri, G., Corsi, D., Cavi, N., Gastaldi, D., et al. (2021). Strategies to Expand the Therapeutic Potential of Superoxide Dismutase by Exploiting Delivery Approaches. *Int. J. Biol. Macromol.* 168, 846–865. doi:10.1016/j.ijbiomac.2020.11.149
- Stockwell, B. R., Jiang, X., and Gu, W. (2020). Emerging Mechanisms and Disease Relevance of Ferroptosis. *Trends Cell Biol.* 30, 478–490. doi:10.1016/j.tcb.2020.02.009
- Sullivan, L. B., Martinez-Garcia, E., Nguyen, H., Mullen, A. R., Dufour, E., Sudarshan, S., et al. (2013). The Proto-Oncometabolite Fumarate Binds Glutathione to Amplify ROS-dependent Signaling. *Mol. Cell* 51, 236–248. doi:10.1016/j.molcel.2013.05.003
- Sun, M., Zhang, J., Liang, S., Du, Z., Liu, J., Sun, Z., et al. (2021). Metabolomic Characteristics of Hepatotoxicity in Rats Induced by Silica Nanoparticles. *Ecotoxicol. Environ. Saf.* 208, 111496. doi:10.1016/j.ecoenv.2020.111496
- Tang, J.-F., Wang, X.-Y., Wen, Q., Tang, S., Sang, F., Li, W.-X., et al. (2017). Idiosyncratic Hepatotoxicity Evaluation of Zhuangguguanjie Wan Mediated by Immune Stress. *Acta Pharm. Sin.* 52, 1033–1040. doi:10.16438/j.0513-4870.2017-0303
- Tang, J., Wang, X., Yang, W., Li, W., Li, Y., Bai, Z., et al. (2018). Cytokine Analysis of Zhuangguguanjie Wan-Induced Idiosyncratic Liver Injury Based on Mathematical Modeling. *Acta Pharm. Sin.* 53, 574–584. doi:10.16438/j.0513-4870.2018-0008
- Tang, D., Chen, X., Kang, R., and Kroemer, G. (2021). Ferroptosis: Molecular Mechanisms and Health Implications. *Cell Res.* 31, 107–125. doi:10.1038/s41422-020-00441-1
- Thévenot, E. A., Roux, A., Xu, Y., Ezan, E., and Junot, C. (2015). Analysis of the Human Adult Urinary Metabolome Variations with Age, Body Mass Index, and Gender by Implementing a Comprehensive Workflow for Univariate and OPLS Statistical Analyses. *J. Proteome Res.* 14, 3322–3335. doi:10.1021/acs.jproteome.5b00354
- Tujios, S., and Fontana, R. J. (2011). Mechanisms of Drug-Induced Liver Injury: from Bedside to Bench. *Nat. Rev. Gastroenterol. Hepatol.* 8, 202–211. doi:10.1038/nrgastro.2011.22
- Ursini, F., and Maiorino, M. (2020). Lipid Peroxidation and Ferroptosis: The Role of GSH and GPx4. *Free Radic. Biol. Med.* 152, 175–185. doi:10.1016/j.freeradbiomed.2020.02.027
- Vabulas, R. M. (2021). Ferroptosis-Related Flavoproteins: Their Function and Stability. *Int. J. Mol. Sci.* 22, 430. doi:10.3390/ijms22010430
- Wang, J. B., Kong, W. J., Wang, H. J., Zhao, H. P., Xiao, H. Y., Dai, C. M., et al. (2011). Toxic Effects Caused by Rhubarb (*Rheum Palmatum* L.) Are Reversed on Immature and Aged Rats. *J. Ethnopharmacol.* 134, 216–220. doi:10.1016/j.jep.2010.12.008
- Wang, F., Liu, Y., Yuan, J., Yang, W., and Mo, Z. (2019). Compound C Protects Mice from HFD-Induced Obesity and Nonalcoholic Fatty Liver Disease. *Int. J. Endocrinol.* 2019, 3206587. doi:10.1155/2019/3206587
- Wang, H., Liu, C., Zhao, Y., and Gao, G. (2020). Mitochondria Regulation in Ferroptosis. *Eur. J. Cell Biol.* 99, 151058. doi:10.1016/j.ejcb.2019.151058
- Wang, Z., Xu, G., Wang, H., Zhan, X., Gao, Y., Chen, N., et al. (2020). Icariside II, a Main Compound in Epimedium Folium, Induces Idiosyncratic Hepatotoxicity by Enhancing NLRP3 Inflammasome Activation. *Acta Pharm. Sin. B* 10, 1619–1633. doi:10.1016/j.apsb.2020.03.006
- Wu, W., Wang, T., Sun, B., Liu, D., Lin, Z., Miao, Y., et al. (2019). Xian-Ling-Gu-Bao Induced Inflammatory Stress Rat Liver Injury: Inflammatory and Oxidative Stress Playing Important Roles. *J. Ethnopharmacol.* 239, 111910. doi:10.1016/j.jep.2019.111910
- Xie, X., Zhao, Y., Ma, C. Y., Xu, X. M., Zhang, Y. Q., Wang, C. G., et al. (2015). Dimethyl Fumarate Induces Necroptosis in Colon Cancer Cells through GSH Depletion/ROS increase/MAPKs Activation Pathway. *Br. J. Pharmacol.* 172, 3929–3943. doi:10.1111/bph.13184
- Xie, Y., Hou, W., Song, X., Yu, Y., Huang, J., Sun, X., et al. (2016). Ferroptosis: Process and Function. *Cell Death Differ.* 23, 369–379. doi:10.1038/cdd.2015.158
- Yan, B., Ai, Y., Sun, Q., Ma, Y., Cao, Y., Wang, J., et al. (2021). Membrane Damage during Ferroptosis Is Caused by Oxidation of Phospholipids Catalyzed by the Oxidoreductases POR and CYB5R1. *Mol. Cell* 81, 355. doi:10.1016/j.molcel.2020.11.024
- Yang, W. S., and Stockwell, B. R. (2016). Ferroptosis: Death by Lipid Peroxidation. *Trends Cell Biol.* 26, 165–176. doi:10.1016/j.tcb.2015.10.014

- Yuan, H., Li, X., Zhang, X., Kang, R., and Tang, D. (2016). Identification of ACSL4 as a Biomarker and Contributor of Ferroptosis. *Biochem. Biophys. Res. Commun.* 478, 1338–1343. doi:10.1016/j.bbrc.2016.08.124
- Zhang, A., Sun, H., Yan, G., Wang, P., and Wang, X. (2016). Mass Spectrometry-Based Metabolomics: Applications to Biomarker and Metabolic Pathway Research. *Biomed. Chromatogr.* 30, 7–12. doi:10.1002/bmc.3453
- Zhang, L., Zhang, J., Fan, Q., Su, Z., Chen, C., Peng, L., et al. (2018). Hepatotoxicity of Epimedium Folium in Rat Model Based on Uniform Design and Regression Analysis. *Chin. J. Exp. Traditional Med. Formulae* 24, 189–197. doi:10.13422/j.cnki.syfjx.20180617
- Zhang, Z., Yang, L., Huang, X., and Gao, Y. (2019). Metabolomics Profiling of Polygoni Multiflori Radix and Polygoni Multiflori Radix Preparata Extracts Using UPLC-Q/TOF-MS. *Chin. Med.* 14, 46. doi:10.1186/s13020-019-0268-3
- Zhang, T., Tsutsuki, H., Islam, W., Ono, K., Takeda, K., Akaike, T., et al. (2021). ATP Exposure Stimulates Glutathione Efflux as a Necessary Switch for NLRP3 Inflammasome Activation. *Redox Biol.* 41, 101930. doi:10.1016/j.redox.2021.101930
- Zhang, L., Xu, A. L., Yang, S., Zhao, B. S., and Wang, T. (2020). In Vitro Screening and Toxic Mechanism Exploring of Leading Components with Potential Hepatotoxicity of Herba Epimedium Extracts. *Toxicol Vitro* 62, 104660. doi:10.1016/j.tiv.2019.104660
- Zhang, Y., Yu, D., Zhang, J., Bao, J., Tang, C., and Zhang, Z. (2020). The Role of Necroptosis and Apoptosis through the Oxidative Stress Pathway in the Liver of Selenium-Deficient Swine. *Metallomics* 12, 607–616. doi:10.1039/c9mt00295b
- Zhong, R., Chen, Y., Ling, J., Xia, Z., Zhan, Y., Sun, E., et al. (2019). The Toxicity and Metabolism Properties of Herba Epimedium Flavonoids on Laval and Adult Zebrafish. *Evid. Based Complement. Altern. Med.* 2019, 3745051. doi:10.1155/2019/3745051

Conflict of Interest: The authors declare that the research was conducted in the absence of any commercial or financial relationships that could be construed as a potential conflict of interest.

Publisher's Note: All claims expressed in this article are solely those of the authors and do not necessarily represent those of their affiliated organizations or those of the publisher, the editors, and the reviewers. Any product that may be evaluated in this article, or claim that may be made by its manufacturer, is not guaranteed or endorsed by the publisher.

Copyright © 2022 Li, Zhang, Guo, Kang, Chen, Liu, Ma, Zhang, Hu and Wang. This is an open-access article distributed under the terms of the Creative Commons Attribution License (CC BY). The use, distribution or reproduction in other forums is permitted, provided the original author(s) and the copyright owner(s) are credited and that the original publication in this journal is cited, in accordance with accepted academic practice. No use, distribution or reproduction is permitted which does not comply with these terms.